Manipulation of the Majorana Fermion, Andreev Reflection, and Josephson Current on Topological Insulators

Yukio Tanaka,[1] Takehito Yokoyama,[2] and Naoto Nagaosa[2,3]
[1]*Department of Applied Physics, Nagoya University, Nagoya, 464-8603, Japan*
[2]*Department of Applied Physics, University of Tokyo, Tokyo 113-8656, Japan*
[3]*Cross Correlated Materials Research Group (CMRG), ASI, RIKEN, WAKO 351-0198, Japan*
(Received 10 July 2009; published 4 September 2009)

We study theoretically the transport properties of a normal metal (N)/ferromagnet insulator (FI)/superconductor (S) junction and a S/FI/S junction formed on the surface of a three-dimensional topological insulator, where the chiral Majorana mode exists at the FI/S interface. We find the chiral Majorana mode generated in N/FI/S and S/FI/S junctions is very sensitively controlled by the direction of the magnetization $\boldsymbol{m}$ in the FI region. In particular, the current-phase relation of the Josephson current in S/FI/S junctions has a phase shift of neither 0 nor π that can be tuned continuously by the component of $\boldsymbol{m}$ perpendicular to the interface.

DOI: 10.1103/PhysRevLett.103.107002 PACS numbers: 74.45.+c, 71.10.Pm, 74.90.+n

A class of time-reversal symmetric insulators with nontrivial topological properties has been proposed theoretically and discovered experimentally [1–3]. The hallmark of this insulator, i.e., a topological insulator (TI), is the edge or surface channels, while the bulk states are gapped. In the two-dimensional (2D) case, helical modes appear at the edge of the sample, i.e., the pair of one-dimensional modes connected by the time-reversal symmetry and propagating in the opposite directions for opposite pseudospins [2]. This is analogous to the chiral edge modes in the quantum Hall systems [4]. Therefore, the TI in the 2D case can be regarded as two copies of the quantum Hall systems for up and down pseudospins [5], and is often called the quantum spin Hall system. In the three-dimensional (3D) case, there are two classes of TIs, i.e., weak TIs (WTIs) and strong TIs (STIs), corresponding to the even (WTI) and odd (STI) number of the chiral Dirac fermions on the surface [6]. Since the even number of Dirac fermions can be paired to open the gap, those in WTIs are fragile against the disorder and/or the interactions, while they are robust in STIs. The 2D quantum spin Hall system is adiabatically continued to the WTI when the weak interlayer coupling is tuned, while the STI has no analogue to the quantum Hall system, and is a genuine new state of matter.

The 2D chiral Dirac fermion on the surface of the STI is protected by the bulk gap and its topological property. Therefore, it offers an interesting system to look for the 2D superconductivity with the Cooper pairs mediated by the bosonic excitations, e.g., phonons and excitons, in the STI. Fu and Kane studied the superconductivity induced by the proximity effect to the surface of the STI [7]. Considering the interface between the ferromagnetic insulator (FI) and conventional superconductor (S), they predicted the appearance of the chiral Majorana state as an Andreev bound state [7]. We call this the chiral Majorana mode (CMM), which has a dispersion along the interface while it is confined along the direction perpendicular to the interface. Detecting the Majorana fermions in terms of the interferometry has been proposed also [8,9].

The presence of the CMM is predicted in the $p_x + ip_y$ chiral superconductors [10], e.g., Sr_2RuO_4. However, the control of the chiral domains and manipulation of the edge channels are experimentally difficult [11]. In addition, the $p_x + ip_y$ superconductivity is very fragile against the disorder. Also, the CMMs in the ^{3}He and cold atoms have been studied theoretically [12], but they are neutral systems and charge transport is missing there. Therefore, the present system offers a unique opportunity to study the quantum charge transport specific to the CMM and its control, which is more promising to be realized experimentally. However, its theoretical studies have been limited to focusing on the detection of the Majorana fermion itself [8,9,13].

In this Letter, we study the manipulation of the quantum transport properties associated with Majorana fermions at the interface of the S and FI generated on the surface of a TI. Hereafter, since we concentrate on the STI, we denote the TI instead of the STI for simplicity. We show that the direction of the magnetization $\boldsymbol{m}$ can be used to control the Andreev reflection and Josephson current via the CMM generated in normal metal (N)/FI/S and S/FI/S junctions, offering a unique method for superconducting spintronics.

We consider FI/S and S/FI/S structures formed on the surface of 3D topological insulators as shown in Fig. 1. We concentrate on the situation where the TI below the FI becomes the ferromagnetic insulator due to the exchange coupling. Since the surface state of the TI is metallic, we can regard the configuration shown in Fig. 1(a) as a N/FI/S junction with N($x < 0$), FI($0 < x < d$), and S($x > d$). We also consider the S/FI/S junction as shown in Fig. 1(b) with S($x < 0$), FI($0 < x < d$), and S($x > d$). The interfaces

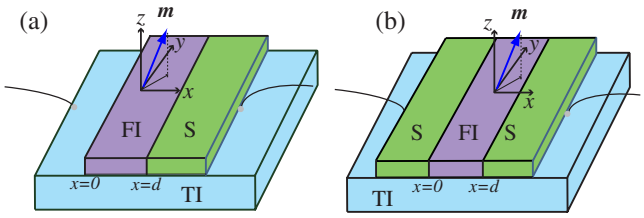

FIG. 1 (color online). Schematic illustration of the junction. (a) N/FI/S junction and (b) S/FI/S junction formed on the surface of a 3D TI. The current is flowing on the surface of the TI.

N(S)/FI and FI/S locate at $x = 0$ and $x = d$, respectively. We assume that the chemical potentials in N and S are equal to each other.

The Hamiltonian of the surface state on the TI is given by

$$\check{H}_{\mathrm{S}} = \begin{pmatrix} \hat{H}(\boldsymbol{k}) + \hat{M} & \hat{\Delta} \\ -\hat{\Delta}^* & -\hat{H}^*(-\boldsymbol{k}) - \hat{M}^* \end{pmatrix} \tag{1}$$

with $\hat{H}(\boldsymbol{k}) = v_{\mathrm{F}}(\hat{\sigma}_x k_x + \hat{\sigma}_y k_y) - \mu[\Theta(-x) + \Theta(x-d)]$, and $\hat{M} = \boldsymbol{m}\cdot\hat{\boldsymbol{\sigma}}\Theta(d-x)\Theta(x)$ with $\boldsymbol{m}\cdot\hat{\boldsymbol{\sigma}} = m_x\hat{\sigma}_x + m_y\hat{\sigma}_y + m_z\hat{\sigma}_z$. Here, μ, $\hat{\boldsymbol{\sigma}}$, v_{F}, $\boldsymbol{m}$ denote chemical potential, Pauli matrices, velocity, and magnetization (times the exchange coupling constant which we assume to be 1), respectively [7]. Note that $\boldsymbol{m}$ enters as an effective vector potential $\boldsymbol{A}$ of the electromagnetic field. The pairing symmetry of the superconductor is assumed to be an s wave, and $\hat{\Delta}$ is given as $\hat{\Delta} = i\hat{\sigma}_y\Delta\Theta(x-d)$ and $\hat{\Delta} = i\hat{\sigma}_y[\Delta\Theta(x-d) + \Delta\Theta(-x)\exp(i\varphi)]$ for N/TI/S and S/TI/S junctions, respectively, where φ denotes the macroscopic phase difference between left and right superconductors. In general, the magnitude of Δ is smaller than that of the bulk energy gap of a superconductor deposited on a TI due to the nonideal S/TI interface [14].

First, let us consider the N/FI/S junction [Fig. 1(a)]. A wave function of an electron injected from N with an injection angle θ is given as $\Psi_{\mathrm{T}} = \exp(ik_y y)[\Psi_{\mathrm{N}}(x)\Theta(-x) + \Psi_{\mathrm{FI}}(x)\Theta(x)\Theta(d-x) + \Psi_{\mathrm{S}}^{\mathrm{R}}(x)\Theta(x-d)]$, where $k_y = k_{\mathrm{F}}\sin\theta$ is the momentum parallel to the interface with $v_{\mathrm{F}}k_{\mathrm{F}} = \mu$. Quasiparticle energy E is measured from μ. $\Psi_{\mathrm{N}}(x)$, $\Psi_{\mathrm{FI}}(x)$, and $\Psi_{\mathrm{S}}^{\mathrm{R}}(x)$ are given by

$$\Psi_{\mathrm{N}}(x) = [(\Psi_{\mathrm{in}} + a\Psi_{\mathrm{hr}})\exp(ik_x x) + b\Psi_{\mathrm{er}}\exp(-ik_x x)], \tag{2}$$

$$\Psi_{\mathrm{FI}}(x) = [\Psi_{e1}\exp(-\tilde{\kappa}_{ex}x) + \Psi_{e2}\exp(\tilde{\kappa}_{ex}^* x) + \Psi_{h1}\exp(\tilde{\kappa}_{hx}x) + \Psi_{h2}\exp(-\tilde{\kappa}_{hx}^* x)], \tag{3}$$

$$\Psi_{\mathrm{S}}^{\mathrm{R}}(x) = [\Psi_{et}\exp(ik_x x) + \Psi_{ht}\exp(-ik_x x)], \tag{4}$$

with $k_x = \sqrt{(\mu/v_{\mathrm{F}})^2 - k_y^2}$, $\tilde{\kappa}_{e(h)x} = \kappa_{e(h)x} + im_x/v_{\mathrm{F}}$, $\kappa_{ex} = \sqrt{m_z^2 + (v_{\mathrm{F}}k_y + m_y)^2}/v_{\mathrm{F}}$, and $\kappa_{hx} = \sqrt{m_z^2 + (v_{\mathrm{F}}k_y - m_y)^2}/v_{\mathrm{F}}$. The four component wave functions ψ_{in}, ψ_{hr}, and ψ_{er} are given by ${}^T\psi_{\mathrm{in}} = (1, \exp(i\theta), 0, 0)$, ${}^T\psi_{\mathrm{hr}} = (0, 0, 1, -\exp(-i\theta))$, ${}^T\psi_{\mathrm{er}} = (1, -\exp(-i\theta), 0, 0)$, with $\exp(i\theta) = (k_x + ik_y)/k_{\mathrm{F}}$. Other wave functions ψ_{e1}, ψ_{e2}, ψ_{h1}, ψ_{h2}, ψ_{et}, and ψ_{ht} are obtained by solving Eq. (1) in a similar way by assuming $|E|, \Delta \ll \mu, |m_z|$.

The coefficients of the Andreev reflection a and normal reflection b are obtained by imposing the boundary condition $\Psi_{\mathrm{N}}(x=0) = \Psi_{\mathrm{FI}}(x=0)$, and $\Psi_{\mathrm{FI}}(x=d) = \Psi_{\mathrm{S}}^{\mathrm{R}}(x=d)$. Then, the angle-resolved tunneling conductance for injection angle θ is obtained by the standard way as $\sigma_{\mathrm{S}}(\theta) = 1 + |a|^2 - |b|^2$. It is noted that $\sigma_{\mathrm{S}}(\theta)$ is not influenced by m_x. The normalized angle-averaged tunneling conductance σ by its value in the normal state is given by [15]

$$\sigma = \frac{\int_{-\pi/2}^{\pi/2}\sigma_{\mathrm{S}}(\theta)\cos\theta d\theta}{\int_{-\pi/2}^{\pi/2}\sigma_{\mathrm{N}}\cos\theta d\theta}. \tag{5}$$

σ_{N} denotes the transparency of the junction in the normal state given by $\sigma_{\mathrm{N}} = 1/[\cosh^2(\kappa_{ex}d) + \tan^2\theta\sinh^2(\kappa_{ex}d)(k_y + m_y/v_{\mathrm{F}})^2/\kappa_{ex}^2]$. First, we focus on the case with $m_y = 0$. In this case, $\sigma_{\mathrm{S}}(\theta)$ can be given by

$$\sigma_{\mathrm{S}}(\theta) = \frac{\sigma_{\mathrm{N}}[1 + \sigma_{\mathrm{N}}|\Gamma|^2 - (1-\sigma_{\mathrm{N}})|\Gamma|^4]}{|1 + (1-\sigma_{\mathrm{N}})\exp(i\gamma)\Gamma^2|^2} \tag{6}$$

with $\exp(i\gamma) = [m_z\cos\theta + i\mu\sin\theta]/[m_z\cos\theta - i\mu\sin\theta]$ and $\Gamma = \Delta/(E + \sqrt{E^2 - \Delta^2})$. For $\sigma_{\mathrm{N}} \to 0$, the denominator of $\sigma_{\mathrm{S}}(\theta)$ becomes zero at $E = E_b$

$$E_b = -\frac{\Delta\mu\sin\theta\,\mathrm{sgn}(m_z)}{\sqrt{\mu^2\sin^2\theta + m_z^2\cos^2\theta}}. \tag{7}$$

This condition coincides with the formation of the CMM at the FI/S interface with semi-infinite S. The CMM and Andreev reflection are strongly related to each other, and $|a| = 1$ is satisfied at $E = E_b$ independent of σ_{N}. It is noted that the sign of E_b is changed by reversing the direction of magnetization m_z. E_b, $\sigma_{\mathrm{S}}(\theta)$, and σ are independent of m_x. As a special limit of $m_z = \mu$, this formula includes the case of the chiral $p_x + i\mathrm{sgn}(-m_z)p_y$-wave superconductor where E_b is reduced to be $E_b = -\Delta\sin\theta\,\mathrm{sgn}(m_z)$ [16], although the given pair potential is a full gap s wave. It is remarkable that the sign of m_z corresponds to the chirality of the CMM, which can be controlled by the direction of magnetization of FI. Here, we focus on the bias voltage V dependence of σ with $E = eV$. As shown in Fig. 2, the resulting σ has a zero bias conductance peak originating from the peak of $\sigma_{\mathrm{S}}(\theta)$ at $E = E_b$. As seen from the left panel of Fig. 2, the slope of the curve of E_b around $E_b = 0$ ($\theta = 0$) becomes gradual with the decrease of μ/m_z. Then, the contribution around $\theta = 0$ becomes significant in the integral of the numerator in Eq. (5), and the resulting height of the zero bias con-

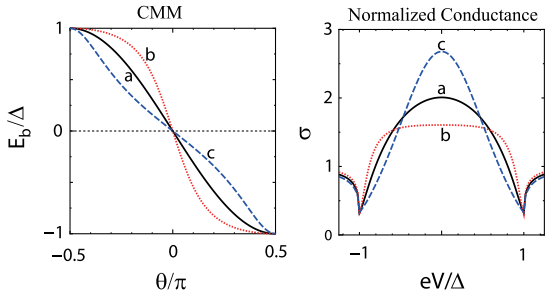

FIG. 2 (color online). Left panel: CMM energy dispersion E_b as a function of the incident angle θ. Right panel: Normalized tunneling conductance σ in N/FI/S junctions. $m_z d/v_F = 1$ and $m_y/m_z = 0$. Curve a represents $\mu/m_z = 1$, b $\mu/m_z = 2$, and c $\mu/m_z = 0.5$.

ductance peak is enhanced with the decrease of the magnitude of μ/m_z as shown in the right panel.

The presence of m_y also influences the CMM as shown in the left panel of Fig. 3. The slope of the curve around $E = 0$ becomes gradual (steep) for the positive (negative) value of m_y. The angle-resolved conductance $\sigma_S(\theta)$ plotted in the right panel of Fig. 3 has a peak corresponding to the CMM and is asymmetric around $\theta = 0$, i.e., $\sigma_S(\theta) \neq \sigma_S(-\theta)$. However, as seen from curves A and B or curves C and D, $\sigma_S(\theta, eV) = \sigma_S(-\theta, -eV)$ is satisfied. Because of this relation, the line shape of resulting angle-averaged σ is symmetric around $eV = 0$ when the average is taken equally between positive and negative θ. However, if we consider ferromagnetic metal with $m_y \neq 0$ as an electrode, we can expect an asymmetric line shape of σ around $eV = 0$ since the shift of k_y by m_y breaks the symmetry between θ and $-\theta$ in the integral of Eq. (5). The present CMM is significantly different from that in the noncentrosymmetric superconductor, where CMM appears as helical edge modes [17]. In the present case, one of the spin-split bands is missing compared with the noncentrosymmetric superconductors.

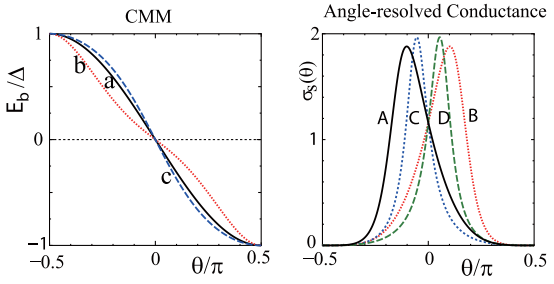

FIG. 3 (color online). Left panel: CMM energy dispersion E_b for curve a $m_y/m_z = 0$, b $m_y/m_z = 0.4$, and c $m_y/m_z = -0.4$. Right panel: $\sigma_S(\theta)$ in N/FI/S junctions. Curve A represents $eV = 0.2\Delta$, $m_y = 0.4m_z$, B $eV = -0.2\Delta$, $m_y = 0.4m_z$, C $eV = 0.2\Delta$, $m_y = -0.4m_z$, and D $eV = -0.2\Delta$, $m_y = -0.4m_z$. In all curves, we choose $m_z d/v_F = 1$ and $\mu/m_z = 1$.

Next, we focus on the Josephson current in the S/FI/S junction [Fig. 1(b)] for $m_y = 0$. Since the magnitudes of the pair potential of the left and right superconductors are equal to each other, it is possible to evaluate the Josephson current by using the CMMs formed in S/FI/S junctions [18]. The CMMs can be obtained as in the case of the N/FI/S junction with wave functions of Eq. (1) under a proper boundary condition. The resulting Josephson current I can be obtained as

$$eIR_N = \frac{\sin(\varphi - 2\delta)\int_{-\pi/2}^{\pi/2} d\theta \frac{\pi\Delta^2 \tanh(E_J/2k_BT)\sigma_N \cos\theta}{2E_J}}{\int_{-\pi/2}^{\pi/2} d\theta \sigma_N \cos\theta}, \quad (8)$$

$$E_J = \sqrt{\sigma_N \cos^2(\varphi/2 - \delta) + (1 - \sigma_N)(E_b/\Delta)^2}\Delta, \quad (9)$$

with resistance in the normal state R_N, $\delta = m_x d/v_F$, and temperature T. The appearance of δ in the current-phase relation stems from the fact that $\tilde{\kappa}_{e(h)x}$ in Eq. (3) becomes complex number in the presence of m_x. The position of the present CMMs in S/FI/S junctions is given by $\bar{E}_b = \pm E_J$. The expression of $\bar{E}_b$ can be explained by the hybridization of two CMMs formed at the left S/FI interface and right FI/S interface. The formula of $\bar{E}_b$ [Eq. (9)] is very general including several preexisting cases. As a special limit with $E_b = \Delta$, and $m_x = 0$, $\bar{E}_b$ is reduced to $\bar{E}_b = \pm\sqrt{\cos^2(\varphi/2) + (1 - \sigma_N)\sin^2(\varphi/2)}\Delta$, which corresponds to the Andreev bound state in a conventional S/nonmagnetic insulator (NI)/S junction [19]. If we choose $E_b = 0$, and $m_x = 0$, the bound state formula in the $d_{xy}(p_x)$-wave /NI/$d_{xy}(p_x)$-wave junction is reproduced [19]. To under-

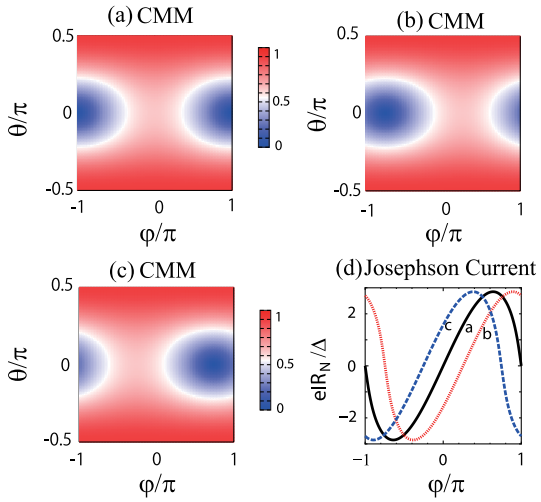

FIG. 4 (color online). Contour plot of CMM energy level E_J as a function of θ and φ for (a) $m_x = 0$, (b) $m_x = 0.4m_z$, (c) $m_x = -0.4m_z$. The resulting Josephson current in S/FI/S junctions is plotted in (d) with curve a representing $m_x/m_z = 1$, b $m_x/m_z = 0.4$, and c $m_x/m_z = -0.4$. In all panels, we choose $m_z d/v_F = 1$, $\mu/m_z = 1$, and $m_y/m_z = 0$. $T = 0.05T_C$ with transition temperature T_C.

stand the θ and φ dependence of $\bar{E}_b$ (E_J) more intuitively, we plot E_J (absolute value of $\bar{E}_b$) in Fig. 4. E_J is an even function of θ for any m_x. For $m_x = 0$, E_J is symmetric with respect to $\varphi = 0$ [Fig. 4(a)]. However, for $m_x \neq 0$, the resulting E_J is no more symmetric around $\varphi = 0$ as shown in Figs. 4(b) and 4(c).

Differently from σ for the Andreev reflection, m_x seriously influences I as the effective vector potential which directly enters into the phase of the Josephson coupling φ. Here, the absence of the small factor of e/c, which reduces the coupling to the magnetic field, makes the tuning of the current-phase relation much easier. Reflecting the φ dependence of E_J, the resulting I becomes zero at neither $\varphi = 0$ nor $\varphi = \pm\pi$ [curves b and c in Fig. 4(d)] due to the presence of the phase shift 2δ. Up to now, there have been many studies about the Josephson current in ferromagnet junctions [20], where the value of phase shift becomes neither 0 nor π in the usual cases. The intermediate phase shift has been predicted in a few cases even in the absence of a Majorana fermion: (i) a spin-singlet-s-wave–spin-triplet-superconducting junction [21]; (ii) an even-frequency–odd-frequency junction [22]; and (iii) a ferromagnet junction with a spin-singlet s-wave superconductor in the presence of the spin-flip scattering or spin-orbit coupling [23,24]. It is remarkable that this anomalous current-phase relation appears by simply controlling one magnetization vector without using unconventional pairing in the present model. It is also noted that the resulting current-phase relation can be continuously tuned by the change of m_x similar to the control of the magnetization vectors at the interfaces of the ferromagnet junction [23]. We hope this anomalous current-phase relation will be detected experimentally in SQUID.

In conclusion, we have studied the charge transport properties of the N/FI/S junction and S/FI/S junction formed on the surface of a three-dimensional (3D) topological insulator, where the CMM exists at the FI/S interface. We have found that CMMs generated in N/FI/S and S/FI/S junctions are controlled by the direction of the magnetization $\boldsymbol{m}$ in the FI region very sensitively. Since the metallic surface state of a 3D topological insulator has been observed experimentally, our proposed structure will be accessible in the near future [25]. Our results provide guidance for innovating a novel direction for superconducting spintronics.

This work is partly supported by Grants No. 20654030, No. 19048015, and No. 19048008 from MEXT, Japan, and NTT basic research laboratories. T. Y. acknowledges support from JSPS.

Note added.—After submission of this Letter, the Majorana fermion in the superconductor/ semiconductor heterostructure was predicted in the presence of the interplay of the spin-orbit coupling and exchange field [26].

[1] C. L. Kane and E. J. Mele, Phys. Rev. Lett. **95**, 146802 (2005); L. Fu and C. L. Kane, Phys. Rev. B **74**, 195312 (2006).
[2] B. A. Bernevig and S. C. Zhang, Phys. Rev. Lett. **96**, 106802 (2006); B. A. Bernevig, T. L. Hughes, and S. C. Zhang, Science **314**, 1757 (2006).
[3] M. König *et al.*, Science, **318**, 766 (2007); M. König *et al.*, J. Phys. Soc. Jpn. **77**, 031 007 (2008).
[4] X. G. Wen, *Quantum Field Theory of Many-Body Systems* (Oxford University Press, Oxford, 2004).
[5] M. Onoda and N. Nagaosa, Phys. Rev. Lett. **95**, 106601 (2005).
[6] L. Fu and C. L. Kane, Phys. Rev. B **76**, 045302 (2007); J. E. Moore and L. Balents, Phys. Rev. B **75**, 121306(R) (2007).
[7] L. Fu and C. L. Kane, Phys. Rev. Lett. **100**, 096407 (2008).
[8] L. Fu and C. L. Kane, Phys. Rev. Lett. **102**, 216403 (2009).
[9] A. R. Akhmerov, J. Nilsson, and C. W. J. Beenakker, Phys. Rev. Lett. **102**, 216404 (2009).
[10] N. Read and D. Green, Phys. Rev. B **61**, 10 267 (2000); D. A. Ivanov, Phys. Rev. Lett. **86**, 268 (2001).
[11] A. P. Mackenzie and Y. Maeno, Rev. Mod. Phys. **75**, 657 (2003); H. Kambara *et al.*, Phys. Rev. Lett. **101**, 267003 (2008).
[12] G. E. Volovik, *The Universe in a Helium Droplet* (Clarendon Press, Oxford, 2003); Y. Tsutsumi *et al.*, Phys. Rev. Lett. **101**, 135302 (2008); S. Tewari *et al.*, Phys. Rev. Lett. **98**, 010506 (2007); M. Sato, Y. Takahashi, and S. Fujimoto, Phys. Rev. Lett. **103**, 020401 (2009).
[13] J. Nilsson, A. R. Akhmerov, and C. W. J. Beenakker, Phys. Rev. Lett. **101**, 120403 (2008).
[14] G. Fagas *et al.*, Phys. Rev. B **71**, 224510 (2005).
[15] C. Bruder, Phys. Rev. B **41**, 4017 (1990); Y. Tanaka and S. Kashiwaya, Phys. Rev. Lett. **74**, 3451 (1995).
[16] M. Yamashiro, Y. Tanaka, and S. Kashiwaya, Phys. Rev. B **56**, 7847 (1997); C. Honerkamp and M. Sigrist, J. Low Temp. Phys. **111**, 895 (1998).
[17] Y. Tanaka *et al.*, Phys. Rev. B **79**, 060505(R) (2009).
[18] C. W. J. Beenakker, Phys. Rev. Lett. **67**, 3836 (1991).
[19] S. Kashiwaya and Y. Tanaka, Rep. Prog. Phys. **63**, 1641 (2000); A. A. Golubov, M. Yu. Kupriyanov, and E. Il'icheve, Rev. Mod. Phys. **76**, 411 (2004).
[20] A. I. Buzdin, Rev. Mod. Phys. **77**, 935 (2005); F. S. Bergeret, A. F. Volkov, and K. B. Efetov, Rev. Mod. Phys. **77**, 1321 (2005).
[21] Y. Asano *et al.*, Phys. Rev. B **67**, 184505 (2003).
[22] Y. Tanaka *et al.*, Phys. Rev. Lett. **99**, 037005 (2007).
[23] R. Grein *et al.*, Phys. Rev. Lett. **102**, 227005 (2009); M. Eschrig *et al.*, J. Low Temp. Phys. **147**, 457 (2007); M. Eschrig and T. Löfwander, Nature Phys. **4**, 138 (2008); Y. Asano *et al.*, Phys. Rev. B **76**, 224525 (2007); V. Braude and Yu. V. Nazarov, Phys. Rev. Lett. **98**, 077003 (2007).
[24] A. Buzdin, Phys. Rev. Lett. **101**, 107005 (2008); F. Konschelle and A. Buzdin, Phys. Rev. Lett. **102**, 017001 (2009).
[25] D. Hsieh *et al.*, Nature (London) **452**, 970 (2008); Science **323**, 919 (2009).
[26] J. D. Sau *et al.*, arXiv:0907.2239.